JOURNAL OF MATERIALS SCIENCE 26 (1991) 5420–5426

Phase diagrams calculated for Fe-rich Fe–Si–Co and Fe–Si–Al ordering alloy systems

MASUHIRO FUKAYA, TORU MIYAZAKI, TAKAO KOZAKAI
Department of Materials Science and Engineering, Nagoya Institute of Technology, Gokiso-cho, Showa-ku, Nagoya 466, Japan

Theoretical analysis based on the calculation of phase diagrams was employed for Fe–Si–Co and Fe–Si–Al ordering systems to clarify the necessity for the occurrence of phase separation in Fe-base ternary ordering systems. The free energy of Fe-base ternary ordering alloys where B2 and $D0_3$ ordered structures are formed is evaluated statistically using a pairwise interaction approximation up to second nearest neighbours, taking into account not only the atomic interaction but also the magnetic interaction, based on the Bragg–Williams–Gorsky model. The calculated phase diagrams are consistent with the experimentally obtained ones. The phase diagram calculation in this work is useful to predict the equilibrium states of the ternary ordering systems. The phase separation in ordering alloys is caused by the contribution of excess free energies due to ordering. The influences of ferromagnetism on the two-phase regions are also demonstrated.

1. Introduction

It has long been recognized that the phase separation of the supersaturated solid solution occurs only in alloy systems with positive interaction parameters between the nearest neighbour atoms. Recently, however, several experimental studies have revealed that the phase separation actually occurs in the ordering solid solutions such as Fe–Al [1–6], Fe–Si [7–10], Cu–Zn [11, 12], Cu–Mn–Al [13], and several Fe-base ternary ordering alloys [14–18], which have negative interaction parameters. The experimental evidence described above has urged us to change the conventional concept that phase separation-type and ordering-type alloys have opposite characteristics for each other.

In order to understand solute atom clustering in ordering alloys, it is important precisely to evaluate the free energies of ordered and disordered solid solutions. For the binary ordering alloys, theoretical approaches [19–38] have been proposed taking into account the interatomic interactions between not only the nearest neighbours but also the second and higher order neighbours. In theoretical treatments of this sort, even if the first-order interaction parameter is negative, phase separations are expected to occur when the second and higher-order interaction parameters are positive.

As regards ternary ordering Fe alloys, we have already found that the two-phase regions exist in the several Fe-rich ternary ordering alloys, and proposed experimental phase diagrams. In the Fe–Si–Co system [16], in addition to A2, B2 and $D0_3$ single-phase regions, the B2 + $D0_3$ two-phase region is found in the two separate composition regions: one is the region connected to the B2 + $D0_3$ region of the Fe–Si binary system; and the other exists in the isolate composition near Fe–15 at% Si–30 at% Co. However, theoretical investigations for the ternary ordering systems are scarce, possibly because of the laborious descriptions of B2 and $D0_3$ ordered structures in the ternary alloys systems.

Recently we proposed the statistical evaluation method of the free energy of Fe-base ternary ordering alloys, where B2 and $D0_3$ ordered structures are formed, and showed the propriety of the evaluation of the free energy [40]. However, for the theoretical justification of experimental results, the calculation of phase diagrams is important.

In the present paper, we firstly show our basic idea for the evaluation of the free energy of Fe-base ternary B2 and $D0_3$ ordered structures [40]. Secondly applying the proposed free energy model on both Fe–Si–Co and Fe–Si–Al ordering systems, we calculate these phase diagrams. Lastly, we account for the occurrence of the phase separation in Fe-base ternary B2 and $D0_3$ ordering solid solutions.

2. Theoretical basis

In order to describe the atomic configurations of B2 and $D0_3$ ordered structures in bcc ternary alloy, the unit cell of the $D0_3$ superlattice is divided into four fcc sublattices I, II, III and IV, as illustrated in Fig. 1. The atoms in sublattices I and II are the nearest neighbours (nn) to the atoms in sublattices III and IV. The atoms in the I or III sublattices are the second nearest neighbours (nnn) to the atoms in II or IV, respectively. To describe the various atomic configurations in the first and second coordination spheres of the bcc ternary alloys, we use six independent parameters defined by occupation probabilities P_i^{ν} of i atom

0022–2461/91 $03.00 + .12

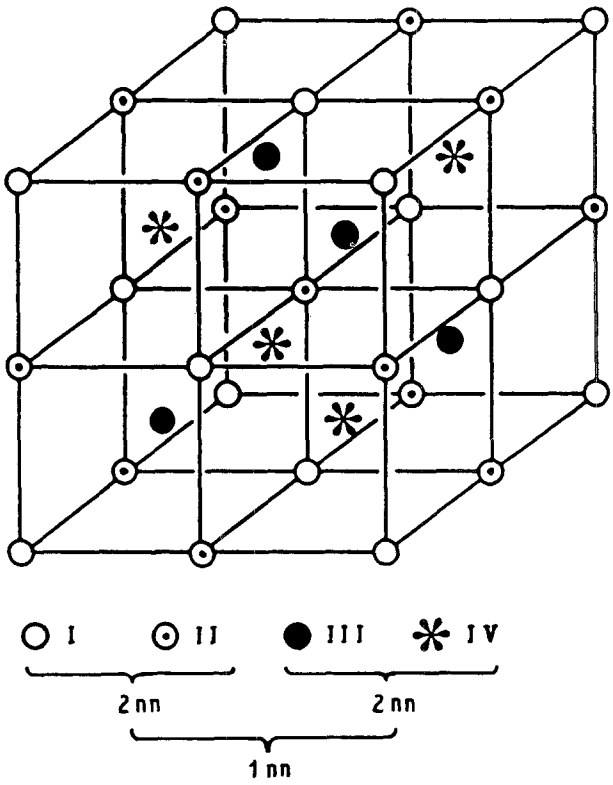

Figure 1 Unit cell of $D0_3$ structure and four f c c sublattices, indicating the nearest (nn) and second nearest (nnn) neighbourhood between atom sites of the sublattices I, II, III, IV.

(i = A, B) in the sublattice L(= I, II, III, IV) as in the case of binary alloys [22, 27].

$$\begin{aligned} X_A &= (P_A^I + P_A^{II} - P_A^{III} - P_A^{IV})/ \\ &\quad (P_A^I + P_A^{II} + P_A^{III} + P_A^{IV}) \\ Y_A &= (P_A^{III} - P_A^{IV})/(P_A^{III} + P_A^{IV}) \\ Z_A &= (P_A^I - P_A^{II})/(P_A^I + P_A^{II}) \\ X_B &= (P_B^I + P_B^{II} - P_B^{III} - P_B^{IV})/ \\ &\quad (P_B^I + P_B^{II} + P_B^{III} + P_B^{IV}) \\ Y_B &= (P_B^{III} - P_B^{IV})/(P_B^{III} + P_B^{IV}) \\ Z_B &= (P_B^I - P_B^{II})/(P_B^I + P_B^{II}) \end{aligned} \quad (1)$$

The parameters X_A and X_B indicate the atomic configurations of A and B atoms between the nearest neighbour sites, i.e. between the sublattices (I + II) and (III + IV). Similarly, other order parameters Y_A, Y_B, Z_A and Z_B show the atomic configurations of A and B atoms between the second nearest neighbour sites, i.e. between the sublattices I and III and also between the sublattices II and IV. All parameters vary in a range of $-1 \leqq X_i, Y_i, Z_i \leqq 1$ (i = A, B). The configurations of C atoms would be inevitably determined by the parameters X_i, Y_i and Z_i (i = A, B). The A2, B2, $D0_3$ and B32 structures of the A–B–C ternary system can generally be expressed by using the six ordering parameters as follows

A2: random distribution atoms in the nn and nnn sites

$$X_A^2 + X_B^2 = 0, \quad Y_A^2 + Y_B^2 + Z_A^2 + Z_B^2 = 0 \quad (2)$$

B2: ordering in the nn and random distribution in the nnn

$$X_A^2 + X_B^2 \neq 0, \quad Y_A^2 + Y_B^2 + Z_A^2 + Z_B^2 = 0 \quad (3)$$

$D0_3$: ordering in the nn and the nnn

$$X_A^2 + X_B^2 \neq 0, \quad Y_A^2 + Y_B^2 + Z_A^2 + Z_B^2 \neq 0 \quad (4)$$

B32: random distribution in the nn and ordering in the nnn

$$X_A^2 + X_B^2 = 0, \quad Y_A^2 + Y_B^2 + Z_A^2 + Z_B^2 \neq 0 \quad (5)$$

The atomic configurations of the ternary ordering structures, defined by Equations 2–5 are related to the electron diffraction patterns experimentally observed [14–18].

The magnetic interactions are derived by considering the pairwise interactions. The magnetic spin is assumed to have just the up or down state, regardless of various values of the actual magnetic moment. Therefore, there are only two separate bond energy states $V_{i\uparrow j\uparrow}^{(1)}$ and $V_{i\uparrow j\downarrow}^{(1)}$ of i–j atom pairs with parallel and antiparallel spins, respectively. The following relations hold:

$$V_{i\uparrow j\uparrow}^{(1)} = V_{i\downarrow j\downarrow}^{(1)} \quad (6)$$

and

$$V_{i\uparrow j\downarrow}^{(1)} = V_{i\downarrow j\uparrow}^{(1)} \quad (7)$$

The higher order of the magnetic interactions such as the second nearest neighbour is neglected. The occupation probabilities of the i atom (i = A, B, C) with up spin or down spin onto the sublattice L(= I, II, III, IV) are given by

$$P_{i\uparrow}^L = P_i^L(1 + q_i)/2 \text{ or } P_{i\downarrow}^L = P_i^L(1 - q_i)/2 \quad (8)$$

respectively, where q_i represents the distribution of magnetic spins, varying in a range of $0 \leqq q_i \leqq 1$. $P_i^L(= P_{i\uparrow}^L + P_{i\downarrow}^L)$ is the probability of existence for the component i in the sublattice L. In Equation 8, $(1 + q_i)/2$ and $(1 - q_i)/2$ are the probabilities of existence for the i atom having up spin and down spin, respectively. The paramagnetic state could be expressed by Equation 9:

$$(1 + q_i)/2 = (1 - q_i)/2 = 0.5 \quad (9)$$

The ferromagnetic and paramagnetic states are shown by $q_i \neq 0$ and $q_i = 0$, respectively.

The atomic interchange energies of the kth neighbours $W_{ij}^{(k)}$ are deduced from the chemical bond energies

$$W_{ij}^{(k)} = -2V_{ij}^{(k)} + V_{ii}^{(k)} + V_{jj}^{(k)} \quad (10)$$

where $V_{ij}^{(k)}$ is the bond energy between atoms i and j in the kth neighbours. The positive $W_{ij}^{(k)}$ corresponds to a larger affinity between the unlike atom pair than the like pair, i.e. the ordering tendency exists. Since the average of the bond energy in the para magnetic i–j crystal is given by

$$V_{ij}^{(1)} = 0.5\{V_{i\uparrow j\uparrow}^{(1)} + V_{i\uparrow j\downarrow}^{(1)}\} \quad (11)$$

the magnetic parameter $J_{ij}^{(1)}$ is defined by Equations 12 and 13:

$$V_{i\uparrow j\uparrow}^{(1)} = V_{ij}^{(1)} + J_{ij}^{(1)} \quad (12)$$

$$V_{i\uparrow j\downarrow}^{(1)} = V_{ij}^{(1)} - J_{ij}^{(1)} \quad (13)$$

In the form of Equations 12 and 13, ferromagnetism occurs when $J_{ij}^{(1)} < 0$. For the sake of simplicity, the magnetic interchange energies $J_{ij}^{(1)}$, as well as the atomic interchange energies $W_{ij}^{(k)}$, are assumed to be independent of temperature, composition and distribution of atoms.

Details of calculations are omitted here, as these have already been reported [40]. The configurational free energy F_k of the A–B–C ternary system containing ferromagnetic elements can be expressed by Equation 14 using a pairwise interaction approximation up to the second nearest neighbours, based on the Bragg–Williams–Gorsky approximation.

$$\begin{aligned}
F_k = {} & U^0 - N\sum_{ij} C_iC_j\{4[W_{ij}^{(1)} + M_{ij}^{(1)}] + 3W_{ij}^{(2)}\} \\
& + 4N\sum_i C_iJ_{ij}^{(1)}q_i^2 \\
& + N\sum_{ij} C_iC_jX_iX_j\{4[W_{ij}^{(1)} + M_{ij}^{(1)}] - 3W_{ij}^{(2)}\} \\
& + 3N/2\sum_{ij} C_iC_j[(1 - X_i)(1 - X_j)Y_iY_j \\
& + (1 + X_i)(1 + X_j)Z_iZ_j]W_{ij}^{(2)} \\
& + k_BNT\sum_i C_i\ln C_i + k_BNT/2\sum_i C_i[(1 - X_i) \\
& \times\ln(1 - X_i) + (1 + X_i)\ln(1 + X_i)] \\
& + k_BNT/4\sum_i\{C_i(1 - X_i)[(1 + Y_i)\ln(1 + Y_i) \\
& + (1 - Y_i)\ln(1 - Y_i)] \\
& + C_i(1 + X_i)[(1 + Z_i)\ln(1 + Z_i) \\
& + (1 - Z_i)\ln(1 - Z_i)]\} \\
& - k_BNT\sum_i m_iC_i\{\ln(8 - 6q_i + 2\sqrt{4 - 3q_i^2}) \\
& - (1 + q_i)\ln(q_i + \sqrt{4 - 3q_i^2}) \\
& - (1 - q_i)\ln[2(1 - q_i)]\}
\end{aligned}$$

where

$$U^0 = N\left\{4\sum_i C_iV_{ii}^{(1)} + 3\sum_i C_iV_{ii}^{(2)}\right\};$$

$$M_{ij}^{(1)} = -2J_{ij}^{(1)}q_iq_j + J_{ii}^{(1)}q_i^2 + J_{jj}^{(1)}q_j^2;$$

$$ij = \text{AB, BC, CA;} \quad i = \text{A, B, C}$$

$$\begin{aligned}
m_A = m_B = m_C = 1 \quad & \text{if } J_{AA}^{(1)} \neq 0, J_{BB}^{(1)} \neq 0, \\
& J_{CC}^{(1)} \neq 0 \\
m_A = 0 \quad & \text{if } J_{AA}^{(1)} = 0 \\
m_B = 0 \quad & \text{if } J_{BB}^{(1)} = 0 \\
m_C = 0 \quad & \text{if } J_{CC}^{(1)} = 0 \quad (14)
\end{aligned}$$

where m_i = a parameter to qualify the ferromagnetic energy with the i-element, which is usually unit in the case where i is a ferromagnetic element; N = Avogadro's number (the number of all lattice sites); C_i = atomic concentration of i; k_B = Boltzman's constant; T = temperature.

3. Calculation of phase diagrams

3.1. Calculated phase diagram of the Fe–Si–Co system

The numerical values [41] used for the calculations are listed in Table I. Fig. 2 shows a calculated phase diagram of the Fe–Si–Co system at 923 K. The solid curves, fine solid straight lines and chain line show phase boundaries, tie-lines of phase separation and iso-Curie temperature curve at 923 K, respectively. There is a B2 + $D0_3$ two-phase coexistent region, as well as A2, B2 and $D0_3$ single-phase regions. The B2 + $D0_3$ two-phase region connects to the B2 + $D0_3$ region of the Fe–Si binary system, and exists up to the composition region over the high Co content alloy of 30 at% Co. The directions of the tie-line of phase separation are almost parallel to the Fe–Si binary system. The two-phase region exists on the boundary between the B2 and $D0_3$ single phase.

3.2. Calculated phase diagram of the Fe–Si–Al system

The numerical values [7, 41] used for the calculations are listed in Table II. In these parameters the exchange energies of the Si–Al system $W_{SiAl}^{(1)}$ and $W_{SiAl}^{(2)}$ were

TABLE I Numerical values for the Fe–Si–Co system

Atomic interchange energy	Value × k_B
$W_{FeSi}^{(1)}$	2010
$W_{FeCo}^{(1)}$	410
$W_{SiCo}^{(1)}$	2600
$W_{FeSi}^{(2)}$	1000
$W_{FeCo}^{(2)}$	0
$W_{SiCo}^{(2)}$	700
$J_{FeFe}^{(1)}$	− 196
$J_{CoCo}^{(1)}$	− 261
$J_{FeCo}^{(1)}$	− 296

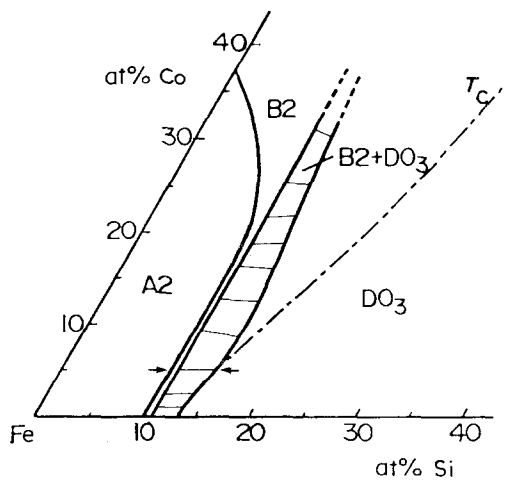

Figure 2 A calculated section phase diagram of the Fe-rich Fe–Si–Co ternary system at 923 K.

TABLE II Numerical values for the Fe–Si–Al system

Atomic interchange energy	Value $\times k_B$
$W^{(1)}_{FeSi}$	2010
$W^{(1)}_{FeAl}$	1120
$W^{(1)}_{SiAl}$	− 1170
$W^{(2)}_{FeSi}$	1000
$W^{(2)}_{FeAl}$	560
$W^{(2)}_{SiAl}$	− 220
$J^{(1)}_{FeFe}$	− 196

evaluated in this work. We performed numerical calculations of the configurational diagrams using the critical temperature equations of A2/B2 and B2/DO_3 so as to regain the A2/B2 and B2/DO_3 transition curves in the experimentally determined phase diagram of the Fe–Si–Al system at 1273 K [14]. The critical temperature equations for both A2/B2 and B2/DO_3 in the ternary system are shown.

The condition for the A2/B2 phase transition is as follows.

$$\left(\frac{\partial^2 F_k}{\partial X_A^2}\right)\left(\frac{\partial^2 F_k}{\partial X_B^2}\right) - \left(\frac{\partial^2 F_k}{\partial X_A \partial X_B}\right)^2 \Bigg|_{\substack{X_A = X_B = Y_A = 0 \\ Y_B = Z_A = Z_B = 0}} = 0 \tag{15}$$

For the B2/DO_3 phase transition is as follows.

$$\left(\frac{\partial^2 F_k}{\partial Z_A^2}\right)\left(\frac{\partial^2 F_k}{\partial Z_B^2}\right) - \left(\frac{\partial^2 F_k}{\partial Z_A \partial Z_B}\right)^2 \Bigg|_{\substack{X_A = X_{A\min},\ X_B = X_{B\min} \\ Y_A = Y_B = Z_A = Z_B = 0}} = 0 \tag{16}$$

Therefore the A2/B2 critical temperature T_{nn} is given in the following equation.

$$k_B T_{nn} = \sum_{ij} C_i C_j \Omega_{ij} + \sqrt{(C_i C_j \Omega_{ij})^2 - C_A C_B C_C (4\Omega_{BC}\Omega_{CA} - [\Omega_{AB} - \Omega_{BC} - \Omega_{CA}]^2)} \tag{17}$$

where $\Omega_{ij} = 4W^{(1)}_{ij} - 3W^{(2)}_{ij}$; and ij = AB, BC, CA. Furthermore, the B2/DO_3 critical temperature T_{nnn} is given in the following equation.

$$k_B T_{nnn} = 3\left\{\Omega + \sqrt{\Omega^2 + C_A C_B (1 + X_A)(1 + X_B)(C_A X_A + C_B X_B - C_C)\,[4W^{(2)}_{BC} W^{(2)}_{CA} - (W^{(2)}_{AB} - W^{(2)}_{BC} - W^{(2)}_{CA})^2]}\right\} \tag{18}$$

where $\Omega = W^{(2)}_{CA} C_A (1 + X_A)(-C_A X_B + X_B + C_C) + W^{(2)}_{BC} C_B (1 + X_B)(C_A - C_B X_B + C_C) + (W^{(2)}_{AB} - W^{(2)}_{BC} - W^{(2)}_{CA}) C_A C_B (1 + X_A)(1 + X_B)$.

Fig. 3 is a calculated phase diagram of the Fe–Si–Al system at 873 K. In the figure the solid curve, fine solid lines and a chain line show the phase boundaries, tie-lines of phase separation and iso-Curie temperature, respectively. The DO_3 single phase exists in a widespread region of the Fe-rich ternary system. The B2 + DO_3 two-phase region exists as a band-shaped region on the boundary between the B2 and DO_3 phases. This B2 + DO_3 two-phase region connects to the B2 + DO_3 region of the Fe–Si binary system and exists up to near the composition region of Fe–2 at% Si–19 at% Al. The directions of the tie-line of phase separation are almost parallel to the Fe–Si binary system.

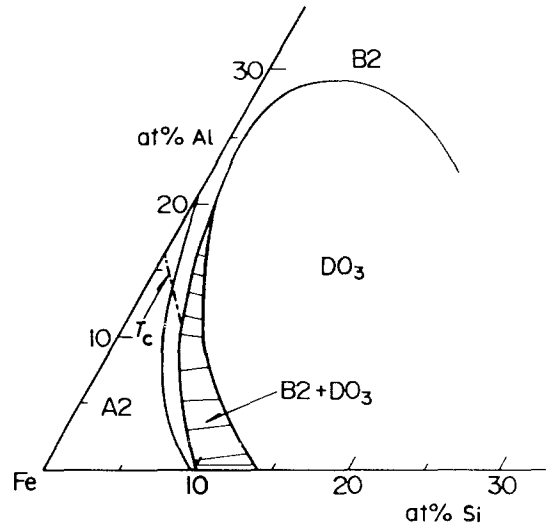

Figure 3 A calculated section phase diagram of the Fe-rich Fe–Si–Al ternary system at 873 K.

4. Discussion

The calculated phase diagrams are compared with the experimentally determined ones. The calculated phase diagram of the Fe–Si–Co system (Fig. 2) has not only A2, B2 and DO_3 single-phase regions but also the B2 + DO_3 coexistent region which connected the B2 + DO_3 region of the Fe–Si binary system with that of a high Co-content alloy. On the other hand, in the experimentally determined phase diagram (Fig. 4) the B2 + DO_3 coexistent region exists in the two separate composition regions: one is the region connected to the B2 + DO_3 region of the Fe–Si binary system; and the other exists in the composition-region near the Fe–13 at% Si–30 at% Co alloy. Therefore there is a little difference between calculation and experiment.

However, it can be said that the calculated phase diagram supports the basic features of the experimental phase diagram, i.e. the composition range of the B2 + DO_3 coexistent region as well as that of the A2, B2 and DO_3 single-phase regions.

In the calculated phase diagram of the Fe–Si–Al system (Fig. 3) the B2 + DO_3 coexistent region exists as a narrow band connecting to the B2 + DO_3 coexistent region of the Fe–Si binary system, and continues up to the alloys near the Fe–Al binary system. On the other hand, in the experimentally determined phase diagram (Fig. 5) a phase change from the B2 + DO_3 of the Fe–Si system to the A2 + DO_3 of the Fe–Al system appears, as the composition shifts from the Fe–Si binary side to the Fe–Al side in the ternary system. This means that the calculation does not succeed the

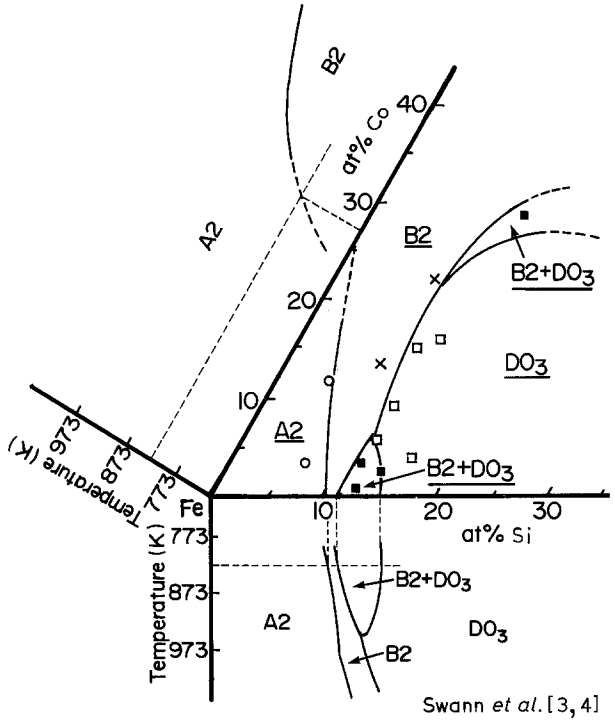

Figure 4 An isothermal section-phase diagram experimentally determined for the Fe-rich Fe–Si–Co ternary system at 823 K [16], together with Fe–Si [10] and Fe–Co [42] binary-phase diagrams. ○, A2 phase; ×, B2 phase; □, DO_3 phase; ■, B2 + DO_3 phase.

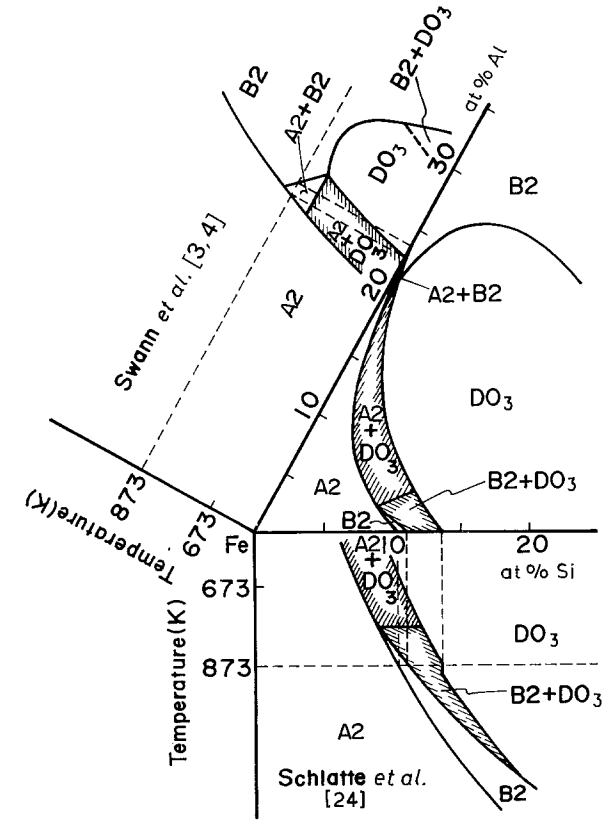

Figure 5 An isothermal section-phase diagram experimentally determined for the Fe-rich Fe–Si–Al ternary system at 873 K [14], together with Fe–Si [24] and Fe–Al [4] binary phase diagrams.

reappearance of the A2 + DO_3 coexistent region near the composition of the Fe–Al binary side. However, the calculated phase diagram (Fig. 3) would support the composition range of the coexistent regions in the Fe–Si–Al ternary system. Therefore an essential difference between calculation and experiment cannot be seen.

As described above the theoretical phase diagrams are nearly identical with the experimental ones. Therefore the free energy evaluation of Fe-base ternary ordering alloys proposed in our previous paper [40], based on a statistical thermodynamic treatment, is considered to be proper and suitable. Furthermore, the theoretical treatment of this work is very useful, as we can easily predict the equilibrium states of Fe-base ternary ordering alloys from just the atomic interchange energies of binary systems constituting the ternary system.

The appearance of the B2 + DO_3 region in the Fe–Si–Co system can be understood by considering the free energies. Fig. 6 gives the free energy curves of the pseudo-binary system along a tie-line (i.e. 5 at% Co) connecting the two points marked by arrows in Fig. 2. The free energy ($F_k - U^0$) can be expressed in Equation 19 as a sum of three terms; chemical free energy (F_{disord}), excess free energy due to ordering ($F_{chem.ord}$), and excess free energy due to magnetism ($F_{mag.ord}$). These are also illustrated in Fig. 6.

$$F_k - U^0 = F_{disord} + F_{chem.ord} + F_{mag.ord} \quad (19)$$

The chemical free energy F_{disord} is always concave. The free energy of A2, F_{A2}, which is the sum of F_{disord} and $F_{mag.ord}$, is always concave so that the phase separation never occurs. That is to say, the magnetic free

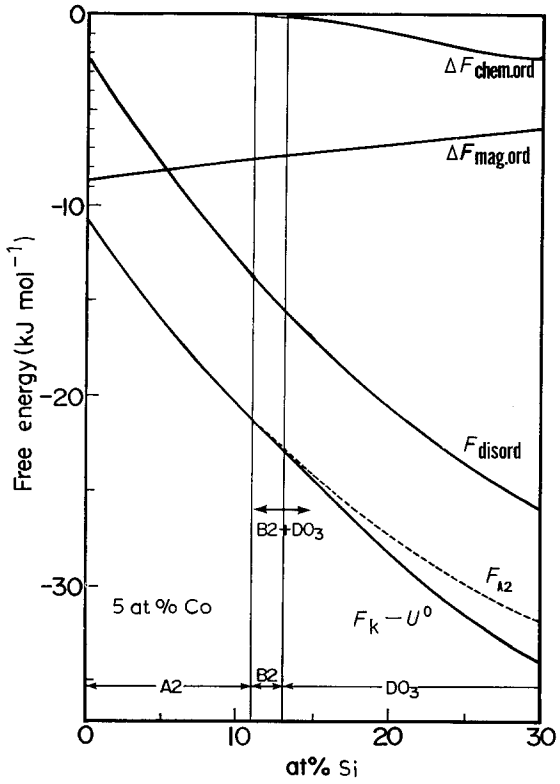

Figure 6 Free energy ($F_k - U^0$) of the most stable atomic configurations of the Fe–Si–Co pseudo-binary system which are indicated along the composition axis fixed 5 at% Co at 923 K. F_{disord} = chemical free energy; $F_{chem.ord}$ = ordering excess free energy; $F_{mag.ord}$ magnetic free energy; $F_k - U^0$ total free energy. $F_k - U^0$ is the sum of F_{disord}, $F_{chem.ord}$ and $F_{mag.ord}$. F_{A2} is the sum of F_{disord} and $F_{chem.ord}$.

energy does not contribute to the appearance of the phase separation itself. However, if $F_{\text{chem.ord}}$ is taken into account, the B2 + $D0_3$ coexistent region appears in the composition region from 11 to 15 at% Si. Therefore it is considered that the appearance of the B2 + $D0_3$ coexistent region in Fe–Si–Co ordering alloys is not due to the influence of ferromagnetism, but is essentially due to the contribution of the excess free energy arising from both B2 and $D0_3$ ordering. Fig. 7 shows the free energy difference ΔF between $(F_k - U^0)$ of Fig. 6 and the common tangent at this function. The difference corresponds to the driving force for phase separation. Both the ferromagnetic state (solid curves) and the paramagnetic state (dotted curves) are shown in the figure. The ferromagnetism not only increases the driving force for phase separation, but also expands the two-phase region. The same results were obtained in calculation of the Fe–Si–Al system. Fig. 8 gives the free energy increase from the common tangent of the pseudo-binary system along a tie-line (i.e. 5 at% Al). The free energy change of the paramagnetic state is also shown by a dotted curve. Similar to the case of the Fe–Si–Co system, the phase separation is caused by the contribution of the excess free energy due to both B2 and $D0_3$ ordering. The ferromagnetism not only increases the driving force for phase separation, but also expands the two-phase region.

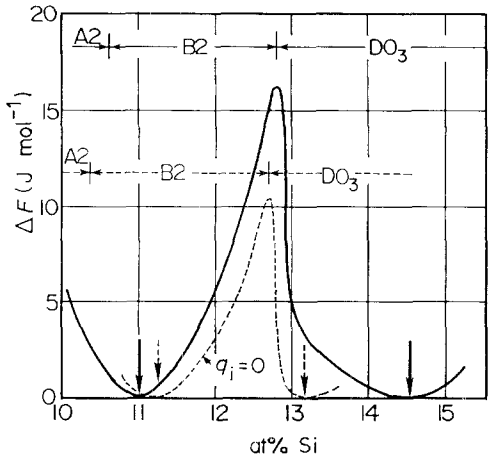

Figure 7 Difference ΔF between $(F_k - U^0)$ of Fig. 6, and the tangent at this function which is common to two points, marked by arrows. The dashed curve (– – –) for paramagnetic crystals can be compared with the solid curve (——) for ferromagnetic crystals at 923 K. Transitions from A2 to B2 configurations and from B2 to $D0_3$ configurations are also indicated.

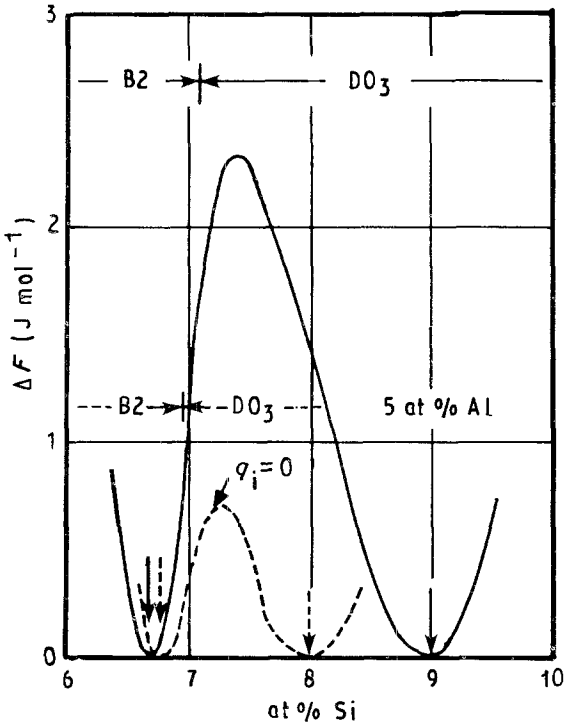

Figure 8 Difference ΔF between $(F_k - U^0)$ and the tangent at this function which is common to two points, marked by arrows. The dashed curve (– – –) for paramagnetic crystals can be compared with the solid curve (——) for ferromagnetic crystals. Transition from B2 to $D0_3$ configuration is also indicated. $T = 873$ K.

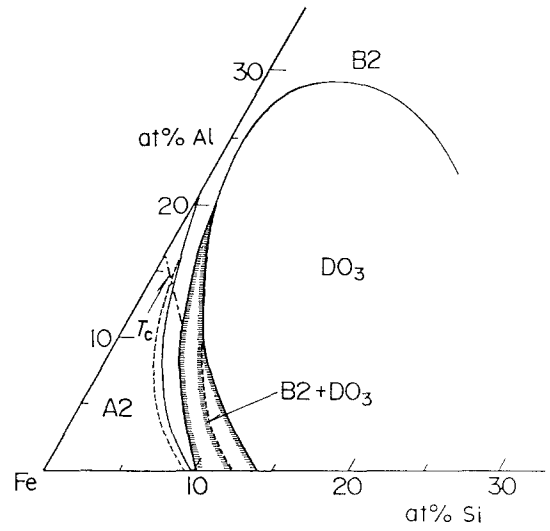

Figure 9 The calculated phase diagrams of both paramagnetic (– – –) and ferromagnetic (——) states, respectively, at 873 K, to demonstrate the influence of ferromagnetism on phase separation.

We show this effect of ferromagnetism on the phase diagram. Fig. 9 shows the calculated phase diagram of the Fe–Si–Al system at 873 K. Phase boundaries of the two-phase region in the paramagnetic state are shown by dotted curves. The two-phase coexistent region expands greatly, especially in the $D0_3$ phase side, due to the influence of the ferromagnetism.

5. Conclusions

In this paper, theoretical analysis based on the calculation of phase diagrams was performed to clarify the necessity for the occurrence of phase separation in Fe-base ternary ordering systems. The results obtained are as follows.

1. The free-energy model based upon the Bragg–Williams–Gorsky approximation was applied to both the Fe–Si–Co and Fe–Si–Al ordering systems, and phase diagrams were calculated. The calculated phase diagrams were consistent with experimentally determined ones. Therefore the theoretical analysis based on the statistical thermodynamic treatment in this work is useful, as we can easily predict the phase equilibrium of actual ternary ordering systems from

only the atomic interaction parameters of three binary systems constituting the ternary system.

2. The phase separation in the ternary ordering system is caused by the contribution of excess free energies due to ordering.

3. The ferromagnetism has the great effect on the expansion of the two-phase region.

Acknowledgements

This work was financially supported in part by a Grant-in-Aid for Scientific Research from the Ministry of Education, Science and Culture, Japan.

References

1. S. M. ALLEN and J. W. CAHN, *Acta Metall.* **23** (1975) 1017.
2. S. M. ALLEN, *Phil. Mag.* **36** (1977) 181.
3. P. R. SWANN, W. R. DUFF and R. M. FISHER, *Trans. Metall. Soc. AIME.* **245** (1969) 851.
4. *Idem, Metall. Trans.* **3** (1972) 409.
5. K. OKI, H. SAGANE and T. EGUCHI, *Jpn J. Appl. Phys.* **13** (1974) 753.
6. H. SAGANE, K. OKI and T. EGUCHI, *Trans. Jpn Inst. Metals* **18** (1977) 488.
7. G. INDEN and W. PITSCH, *Z. Metallkde* **63** (1972) 253.
8. H. H. ETTWIG and W. PEPPERHOFF, *ibid.* **63** (1972) 453.
9. G. SCHLATTE and W. PITSCH, *ibid.* **66** (1975) 660.
10. P. R. SWANN, L. GRÅNÄS and B. LEHTINEN, *Metal Sci.* **9** (1975) 90.
11. H. KUBO and C. M. WAYMAN, *Metall. Trans.* **10A** (1979) 633.
12. H. KUBO, I. CORNELIS and C. M. WAYMAN, *Acta Metall.* **28** (1980) 405.
13. M. BOUCHARD and G. THOMAS, *ibid.* **23** (1975) 1485.
14. T. MIYAZAKI, T. KOZAKAI and T. TSUZUKI, *J. Mater. Sci.* **21** (1986) 2557.
15. T. MIYAZAKI, K. ISOBE, T. KOZAKAI and M. DOI, *Acta Metall.* **35** (1987) 317.
16. M. FUKAYA, T. KOZAKAI and T. MIYAZAKI, *J. Jpn Inst. Metal.* **52** (1988) 369 (in Japanese).
17. S. MATSUMURA, A. SONOBE, K. OKI and T. EGUCHI, in Proceedings of an International Conference on Phase Transformations in Solids, Vol. 21 (Elsevier, New York, 1984) p. 269.
18. M. G. MENDIRATTA, S. K. EHLERS and H. A. LIPSITT, *Metall. Trans.* **18A** (1987) 509.
19. P. Z. ZHAO, T. KOZAKAI and T. MIYAZAKI, *J. Jpn Inst. Metal.* **53** (1989) 266 (in Japanese).
20. P. S. RUDMAN, *Acta Metall.* **8** (1960) 321.
21. W. C. RICHARDS and J. W. CAHN, *ibid.* **19** (1971) 1263.
22. S. M. ALLEN and J. W. CAHN, *ibid.* **20** (1972) 423.
23. G. INDEN and W. PITSCH, *Z. Metallkde* **62** (1971) 627.
24. G. SCHLATTE, G. INDEN and W. PITSCH, *ibid.* **65** (1974) 94.
25. G. INDEN and W. PITSCH, *ibid.* **67** (1976) 462.
26. G. INDEN, *Acta Metall.* **22** (1974) 945.
27. *Idem, Z. Metallkde* **66** (1975) 577.
28. *Idem, ibid.* **66** (1975) 648.
29. *Idem, ibid.* **68** (1977) 529.
30. S. V. SEMENOVSKAYA, *Phys. Status Solidi* **64** (1974) 291.
31. S. V. SEMENOVSKAYA and D. M. UMIDOV, *Phys. Status Solidi* **64** (1974) 627.
32. R. KIKUCHI and C. M. VAN BAAL, *Scripta Metall.* **8** (1974) 425.
33. N. S. GOLOSOV and A. M. TOLSTIK, *J. Phys. Chem. Solids* **36** (1975) 899.
34. *Idem, ibid.* **36** (1975) 903.
35. H. INO, *Acta Metall.* **26** (1978) 827.
36. M. HASAKA, *Trans. Jpn Inst. Metals* **21** (1980) 660.
37. H. SAGANE and K. OKI, *ibid.* **21** (1980) 811.
38. H. KUBO and C. W. WAYMAN, *Acta Metall.* **28** (1980) 395.
39. H. KUBO, *J. Phys. Chem. Solids* **44** (1983) 323.
40. M. FUKAYA, T. MIYAZAKI, P. Z. ZHAO and T. KOZAKAI, *J. Mater. Sci.* **25** (1990) 522.
41. G. INDEN, *Phys. Status Solidi* **56** (1979) 177.
42. M. HANSEN, "Constitution on Binary Alloys" (McGraw-Hill, New York, 1958)

Received 5 April 1990
and accepted 15 January 1991